Suppression of the orbital magnetic moment driven by electronic correlations in $Sr_4Ru_3O_{10}$

Filomena Forte,[1,2,*] Lucia Capogna,[3] Veronica Granata,[1,2] Rosalba Fittipaldi,[1,2] Antonio Vecchione,[1,2] and Mario Cuoco[1,2]

[1]*Consiglio Nazionale delle Ricerche, SPIN, Via G. Paolo II 132, I-84084 Fisciano, Italy*

[2]*Dipartimento di Fisica "E.R. Caianiello," Università degli Studi di Salerno, Via G. Paolo II 132, I-84084 Fisciano, Italy*

[3]*Consiglio Nazionale delle Ricerche, IOM OGG, and Institut Laue Langevin, 71 avenue des Martyrs, F-38042 Grenoble, France*

(Received 30 January 2019; revised manuscript received 31 July 2019; published 30 September 2019)

The coupling of spin and orbital degrees of freedom in the trilayer $Sr_4Ru_3O_{10}$ sets a long-standing puzzle due to the peculiar anisotropic coexistence of out-of-plane ferromagnetism and in-plane metamagnetism. Recently, the induced magnetic structure by in-plane applied fields was investigated by means of spin-polarized neutron diffraction, which allowed the extraction of a substantial orbital component of the magnetic densities at Ru sites. It has been argued that the latter is at the origin of the evident layer-dependent magnetic anisotropy, where the inner layers carry larger magnetic momenta than the outer ones. We present a spin-polarized neutron diffraction study in order to characterize the nature of the ferromagnetic state of $Sr_4Ru_3O_{10}$ in the presence of a magnetic field applied along the c axis. The components of the magnetic densities at the Ru sites reveal a vanishing contribution of the orbital magnetic moment which is unexpected for a material system where orbital and spin degeneracies are lifted by spin-orbit coupling and ferromagnetism. We employ a model that includes the Coulomb interaction and spin-orbit coupling at the Ru site to address the origin of the suppression of the orbital magnetic moment. The emerging scenario is that of nonlocal orbital degrees of freedom playing a significant role in the ferromagnetic phase, with a Coulomb interaction that is crucial to making an antialigned orbital moment at short distance, resulting in a ground state with vanishing local orbital moments.

DOI: 10.1103/PhysRevB.100.104440

I. INTRODUCTION

Ruthenium oxide perovskites of the Ruddlesden-Popper (RP) family $A_{n+1}Ru_nO_{3n+1}$ ($n = 1, 2, 3$) are quite unique materials in the realm of transition-metal oxides, changing drastically their electronic and magnetic properties as a function of the number n of RuO_2 layers in the unit cell [1]. A wide variety of collective phenomena has been observed, including unconventional superconductivity ($n = 1$) [2], heavy d-electron masses ($n = 2, 3$) [3], colossal magnetoresistance effects ($n = 2$) [4], and itinerant ferromagnetism and metamagnetism ($n = 3$) [5,6], as well as anomalous ferromagnetism ($n = \infty$) [7]. In those compounds, the extended nature of $4d$ orbitals of the ruthenium ions leads to comparable energies for competing interactions, i.e., crystal field, Hund, spin-orbit, and electron-lattice couplings and p-d hybridization. Moreover, it renders the physical properties highly dependent on the dimensionality n and susceptible to perturbations such as applied magnetic fields and pressure, without the need for chemical doping [8–11].

Recently, the key role played by the orbital physics as it concerns the electronic and magnetic properties of layered ruthenates has been invoked for several Ca- and Sr-based RP compounds. In such systems, the orbital degree of freedom is typically active and has a complex interplay with charge, spin, and lattice degrees of freedom, which turns out to be quite relevant in setting the unconventional superconductivity in Sr_2RuO_4 [2,12], band-dependent Mott metal-insulator transition [13], orbital ordering in Ca_2RuO_4 [14,15], and metamagnetism and correlated effects in $Sr_3Ru_2O_7$ [16,17].

Situated between $n = 2$ and $n = \infty$, $Sr_4Ru_3O_{10}$ is the $n = 3$ member of the Sr-based RP series with triple layers of corner-sharing RuO_6 octahedra separated by SrO rocksalt double layers [18]. It displays complex phenomena ranging from tunneling magnetoresistance and low-frequency quantum oscillations to nonstandard switching behavior. The most intriguing feature, however, is a borderline magnetism: while along the c axis (perpendicular to the Ru-O layers) $Sr_4Ru_3O_{10}$ shows ferromagnetism with a saturation moment of $1.13\,\mu_B$/Ru and a Curie temperature T_c at 105 K, for the field in the ab plane it exhibits a sharp peak in the magnetization at $T^* = 50$ K and a first-order metamagnetic transition. The coexistence of the interlayer ferromagnetism and the intralayer metamagnetism, i.e., the anisotropy in the field response, is not typically encountered in magnetic materials, and it may arise from a peculiar electronic state with two-dimensional Van Hove singularity close to the Fermi level in conjunction with a distinct coupling of the spins to the orbital states and lattice [19–21]. Another important physical aspect emerging in the $Sr_4Ru_3O_{10}$ metamagnetism is provided by the magnetoelastic coupling [22–24]. In particular, direct evidence of a strong spin-lattice interaction was obtained by means of neutron scattering, demonstrating that significant structural changes occur concomitantly with the metamagnetic transition [22].

Recently, it was proposed that a layer-dependent magnetic state may be allowed due to the interplay between octahedral distortions and spin-orbit and Coulomb interactions [25]. In that experiment, a polarized neutron scattering study was

*Corresponding author: filomena.forte@spin.cnr.it

performed in order to analyze the spin and orbital spatial components of the induced magnetization density $M(\mathbf{r})$ with a magnetic field applied in the *ab* plane and in the metamagnetic regime ($B > 2$ T). It was found that there exists a distinct relation between spin and orbital moments and their amplitudes in the unit cell since they are strongly linked to the layers where the electrons are located. Specifically, the inner ruthenium ions in the triple layer have larger spin and orbital magnetic moments than the outer ones. Remarkably, the inner-outer correspondence is robust with respect to temperature variations since it persists even above T_c, thus indicating that these features are intrinsic to the high-field magnetic state.

We present here the outcome of a polarized neutron scattering study on a high-quality single crystal of $Sr_4Ru_3O_{10}$ in the ferromagnetic (FM) regime, i.e., with a strong magnetic field applied along the easy axis (*c* axis). This study is motivated by the need to clarify the nature of the FM phase, in particular the role of the orbital magnetic moment in setting the magnetic properties of this compound within the inequivalent layers of the unit cell. The refinement of our neutron scattering data reveals a vanishing contribution of the orbital component to the magnetic density at Ru sites. Supported by modeling based on an electron-correlated description that includes the coupling between all the relevant spin-orbital degrees of freedom at inequivalent Ru sites, we interpret this evidence as the effect driven by the spin-orbital exchange energy gain in the FM state. In particular, we show that robust short-range antiferro-orbital correlations, developing within the (d_{zx}, d_{yz}) doublet, are responsible for the vanishing of the local orbital moment in the direction of the applied field. The proposed physical mechanism arises from the balance between electronic correlations and kinetic energy in the presence of spin-orbit coupling and the crystal field (CF) splitting set by the tetragonal distortions, which is a common thread in Ru $4d$-electron-based oxides [14]. Remarkably, our analysis demonstrates a tight connection between the character of the orbital angular momentum and the anisotropic magnetic response of $Sr_4Ru_3O_{10}$: while the orbital component of the magnetic moment is suppressed in the case where a longitudinal field is applied, it is substantial and at the origin of the inequivalent intralayer and interlayer magnetic response in the case of an in-plane field [25].

This paper is organized as follows. In Sec. II, we introduce the experimental setup and the polarized beam approach. In Sec. III, we present the experimental results, while Sec. IV is devoted to their interpretation and the description of a theoretical model which is able to explain the quenching of the orbital angular momentum in the high-field magnetic state. In Sec. V we provide the concluding remarks.

II. EXPERIMENTAL METHODOLOGY

Single crystals of $Sr_4Ru_3O_{10}$ were grown in an image furnace as described elsewhere [26]. The samples were cut into small rectangular slices with an average size of $4 \times 4 \times 0.2$ mm^3. Similar samples were used in our previous studies [22,25]. X-ray diffraction, energy and wavelength dispersive spectroscopy, and neutron Laue diffraction were used to fully characterize the structure, quality, and purity of the crystals. Magnetizations measurements on crystals from the same batch identified the FM transition at $T_c \cong 105$ K and a metamagnetic transition at the temperature $T^* \cong 50$ K, when a magnetic field is applied in the *ab* plane. The metamagnetic transition appears for magnetic field up to 2 T [27].

The experiments were carried out at the D9 and D3 diffractometers at the Institute Laue-Langevin in Grenoble. Preliminary neutron diffraction measurements performed at D9 allowed us to determine the structural parameters and the extinction coefficients at $T = 115$ K to use in the following refinement of the magnetic structure. Polarized beam measurements were then performed with the D3 diffractometer. Such a technique is a well-established probe of the magnetization density via the measurement of the flipping ratio R, which is defined as the ratio of the cross sections with neutrons parallel and antiparallel to the applied magnetic field. In this experiment, a magnetic field of 9 T was applied on cooling along the $[00l]$ direction (i.e., the *c* axis), which is the magnetic easy direction for the crystal. Under these conditions, one could be confident that the magnetic moments were completely aligned in the vertical axis, so that the following simplified expression for the flipping ratio is valid [28]:

$$R = \frac{|F_N(\mathbf{K}) - (\gamma r_0/2\mu_B)M(\mathbf{K})|^2}{|F_N(\mathbf{K}) + (\gamma r_0/2\mu_B)M(\mathbf{K})|^2}, \tag{1}$$

where $\gamma r_0 = 5.36 \times 10^{-15}$ m, $\mathbf{K}$ is the scattering vector, $F_N(\mathbf{K})$ is the nuclear structure factor, and $M(\mathbf{K})$ is the reciprocal space magnetization density. Since the number structure factors $F_N(\mathbf{K})$ are known from the crystal structure, from Eq. (1) one can directly get the amplitude of $M(\mathbf{K})$. The real-space magnetization density $\mathbf{M}(\mathbf{r})$ is then extracted by doing the Fourier transform of $M(\mathbf{K})$.

A wavelength of about 0.825 Å was used to measure the scattering in the $[h00/0k0]$ plane with a tilting option for the detector in order to acquire the intensity of many (hkl) reflections with a nonvanishing l index. Since the crystal cell is quite extended along z, $c \sim 28$ Å, values of l up to 13 could be reached.

A radio-frequency coil inserted between the monochromator and the sample was then used to flip the spin state of the incident neutrons so that the intensity of about 65 independent reflections could be measured at three different temperatures: 2, 50, and 120 K in both the up- and down-spin polarizations, with a degree of polarization of 0.94 for each spin channel. A 0.5-mm erbium filter allowed us to reduce higher-order contamination in the incident beam. A Heussler monochromator was also used.

III. SPIN-POLARIZED NEUTRON DIFFRACTION RESULTS

In this section we present the outcome of the polarized neutron diffraction measurements and the resulting magnetization profile resolved within the layers of the unit cell. We follow the standard procedure which was already presented in a previous study [25]. The magnetic moments were refined from the flipping ratios R using the program FULLPROF [29], assuming a spherical approximation for the electron density [30]. The magnetic form factor was expressed in terms of spherical Bessel functions [29], where only the first two terms were

TABLE I. Total and orbital contributions to the magnetic densities at the ruthenium and oxygen sites at the three relevant temperatures of the system, as refined with the program FULLPROF.

	$B \parallel c$					
	2 K		50 K		115 K	
M (units of μ_B)	M_{tot}	M_{orb}	M_{tot}	M_{orb}	M_{tot}	M_{orb}
Ru_{in}	1.75(7)	0.1(2)	1.5(7)	0.1(2)	0.95(7)	0.1(2)
Ru_{out}	1.10(6)	−0.1(1)	1.0(1)	−0.1(1)	0.61(6)	−0.1(1)
O_{bas}	0.15(1)		0.13(1)		0.07(1)	
O_{ap}	0.05(2)		0.04(2)		0.03(1)	
χ^2	1.74		2.60		1.81	

retained, the first corresponding to the total magnetic moment and the second being related to the orbital component, which is expected in light of the moderate spin-orbit coupling in ruthenates. Due to the large unit cell, the refinement procedure was performed by reducing the number of inequivalent Ru ions, which are sorted in two distinct classes: the ruthenium atoms located in the central layer, which are defined as Ru_{in} (inner), and those in the outer layers, which are indicated as Ru_{out} (outer).

It is worth pointing out that the neutron diffraction data acquired on D9 are compatible with two different nuclear structures, the primitive *Pbam* space group which was already adopted in the literature [31] and the face-centered structure, *Acam*. An extended analysis of the data was performed in order to further investigate the crystal symmetry of the sample and also to understand whether the resulting magnetic outcome might be sensitive to the selected space group. However, no significant differences could be obtained in the least-squares refinement of the two models. Moreover, both crystal structures lead to the same results in terms of magnetization densities. Then the *Pbam* space group was adopted, in agreement with our previous paper and other available data in the literature [25].

In Table I, the values of magnetic densities at the ruthenium sites located in the inner and outer octahedra of the triple-layer unit cell are reported, together with those of the oxygens, for the three temperature values of 2, 50, and 120 K. Several important observations can be extracted from the results in Table I. First of all, we observe that the orbital component of the magnetic moment appears to be vanishing in the present field configuration. Indeed, its value is undetectable within the experimental error for all temperatures which have been considered. This result points out a major difference with respect to what was previously found in the case of an in-plane applied field, where a substantial orbital contribution to the magnetic densities was detected at Ru sites [25]. A discussion of the microscopic mechanism leading to this anisotropic orbital quenching in the high-field magnetic states will be presented in the next section. Instead, the contribution of the oxygens in this kind of system is not negligible, as previously reported [25].

Another important observation deals with the layer dependence of the magnetic density, which is graphically depicted in the maps shown in Fig. 1. Those magnetization density maps were calculated in a direct way with the maximum entropy method [28] implemented in the program DYSNOMIA [32], which is now available in the FULLPROF suite. The most likely spin distribution is the one that maximizes the entropy among those which are compatible with the observed magnetic structure factors. The latter were refined with the program FULLPROF.

Our results show that the inner Ru ions carry a larger spin moment with respect to the outer Ru ions and that this order relation is robust against temperature variation. In Fig. 1, the present results ($B \parallel c$) are compared to what was previously reported for $B \parallel ab$ [25]. The most noticeable effect of the field polarization along the c axis is to invert the trend of the magnetization density on the outer ruthenium ions when the temperature is swept across the metamagnetic transition at around 50 K. Indeed, with the field in the *ab* plane, the outer ruthenium ions are more intensely magnetized at 2 K than above T^*.

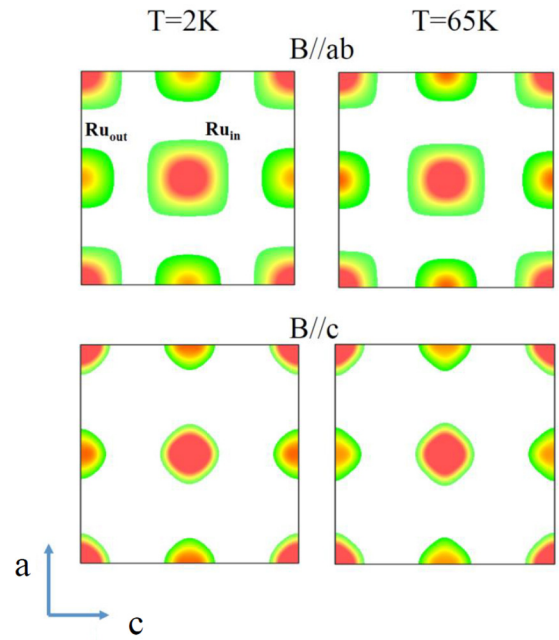

FIG. 1. Sections of the magnetization density in the *ac* plane of $Sr_4Ru_3O_{10}$ calculated directly with the maximum entropy method. The two maps in the top panel are for a sample polarization in the *ab* plane, while the bottom ones correspond to a field applied along the c axis. In the color scale, magnetic density ranges from white (zero magnitude) to red (maximal value at Ru_{in} for $B \parallel c$). For quantitative estimates, refer to the values in Table I.

The inequivalence of the inner and outer ruthenium sites also has crystallographic origins since the inner ruthenium sits in a higher-symmetry site having a Wyckoff position with a multiplicity of 2, while the outer ruthenium has a multiplicity of 4 [31]. In zero field, the outer octahedra are slightly elongated compared to the inner ones, which are regular octahedra [31]. In addition, the inner octahedra are more rotated than the outer ones; in fact, they have an average rotation of 10.6°, while the outer ones 5.25°, with the former being larger than the critical angles, range from 6.5° to 9°, which has been theoretically evaluated to be sufficient to stabilize the ferromagnetism [33]. As a consequence, one can argue that the Ru_{in} are supposed to be more prone to ferromagnetism than the Ru_{out}. This is reflected in the value of FM moment along the c axis on the two sites, which has been measured with neutron scattering at low temperature (2 K), yielding 1.59 μ_B on the inner ruthenium ions and 0.92 μ_B on the outer ones [22]. In the next section, we focus on the role of the orbital component of the magnetic moment and discuss a mechanism which leads to anisotropic suppression, which depends on the orientation of the applied field.

IV. MODELING THE FM STATE WITH A VANISHING ORBITAL MAGNETIC MOMENT

In this section, we propose a physical scenario which is able to account for the occurrence of a vanishing orbital magnetic moment in the high-field FM phase of $Sr_4Ru_3O_{10}$. The analysis is performed by focusing on the orbital character of the spin-polarized ground state described by an effective microscopic model that we solve on a cluster in order to include on equal footing all the interacting electronic degrees of freedom for the d states at the Ru site. The physical context is set by our polarized neutron diffraction study, which reveals a layer-independent quenching of the orbital component of the magnetic density, thus manifesting both at the Ru ions belonging to the central plane and the outer RuO plane of the unit cell, assuming that an external field is applied along the c axis. This result has a completely different outcome and trend compared to the experimental evidence of a substantial orbital component in the magnetic density at the Ru sites, when a field of equal strength is applied along the ab plane [25]. Our aim is to provide a microscopic scenario to account for the realization of a spin-polarized phase with almost zero orbital moment.

On general grounds, the magnetic moment carried by electrons in solid-state materials has two components: the one arising from its spin and the one originating from its orbital character. The local spin magnetic moment typically emerges as a consequence of the Coulomb interaction, and in particular, Hund's coupling is a key player at work in the majority of magnetic solids. On the other hand, concerning the formation of the orbital magnetic moment, it is ascribed to the spin-orbit coupling, which lifts the quenching of the orbital moment in a magnetic solid. Hence, in a FM configuration, where the spin degeneracy is lifted, the spin-orbit coupling (SOC), $H_{\rm soc} = \lambda \mathbf{L} \cdot \mathbf{S}$, is expected to yield an orbital moment $\mathbf{L}$ antiparallel to the spin moment $\mathbf{S}$, with λ being the strength of the SOC. We would then have a local orbital moment at each Ru site along the c axis in the spin-orbit coupled FM state of $Sr_4Ru_3O_{10}$. Hence, another mechanism has to be invoked to account for its suppression. Starting from this picture, we demonstrate that the formation of distinct nonlocal orbital correlations could be the driving mechanism leading to the suppression of the orbital moment. More specifically, a correlated FM state with approximately isotropic short-range antiferrotype orbital configurations, i.e., orbital moments aligning in such a way that they are antiparallel on neighboring sites, can yield a quantum configuration where the average on-site orbital moment is suppressed. In order to proceed further, we introduce a minimal model which is able to capture the competition between the local and nonlocal microscopic mechanisms governing the formation of the magnetic orbital moment. Due to the correlated nature of Ru-based oxides we adopt a standard model Hamiltonian for the itinerant electrons of the t_{2g} Ru bands close to the Fermi level, which includes all the relevant interaction terms at the Ru sites, and the kinetic part for the Ru-Ru connectivity, in the presence of an applied magnetic field. The local Hamiltonian consists of the complete Coulomb interaction for the t_{2g} electrons (i.e., density-density coupling U and Hund interaction J_H), the spin-orbit coupling λ, and the tetragonal CF potential Δ mimicking the static electron-lattice coupling [34]. We face the problem by performing an exact diagonalization study of an effective cluster of two Ru sites. This approach allows us to solve the full quantum Hamiltonian in an unbiased way, so that we can capture the effects of the short-range spin-charge-orbital couplings, which are set by the competition of local interactions and the kinetic energy set by the d-d hopping amplitude t [35]. The details of the microscopic model Hamiltonian are reported in the Appendix.

Concerning the crystal field potential, we observe that positive (negative) values of Δ correspond to an elongated (flat) RuO_6 octahedron along the c axis and favor the occupation in the $d_{xz,yz}$ (d_{xy}) sector. We start by considering as a reference the CF configuration at zero field and assume Δ_1 is negative to simulate Ru_{in} and Δ_2 is positive to simulate Ru_{out}. In a second instance, we will also vary the CF parameters in order to address possible magnetoelastic effects driven by the applied field and to assess the robustness of the obtained effects with respect to the octahedral distortions.

Since we deal with 4d oxides, it is also important to include the atomic spin-orbit coupling, which in several RP ruthenates has strength comparable to the CF splitting among the t_{2g} levels [14,36]. In particular, we adopt the Russel-Saunders scheme suitable for correlated ruthenates [34] and assume that total spin $\mathbf{S_i}$ and orbital angular momentum $\mathbf{L}_{\rm i}$ are formed at the ionic level, which are coupled by the SOC Hamiltonian. Moreover, since the total angular momentum is not a good quantum number, we consider the $\mathbf{S}_{\rm i}$ and $\mathbf{L}_{\rm i}$ components and evaluate the corresponding average expectation values to fully characterize the spin and orbital character of the ground state.

Then, taking into account local-density approximation predictions [1], we assign as a reference in the calculations the values $t = 0.4$ eV and $\Delta_1/t = -0.3$, $\Delta_2/t = 0.225$ for the CF parameters of the central flat and outer elongated octahedra, respectively. Subsequently, we will also vary Δ_2/t from positive to negative values in order to explore different regimes of octahedral distortions. Concerning the Coulomb interactions, we consider the ratio $U/J_H = 5.0$ and analyze

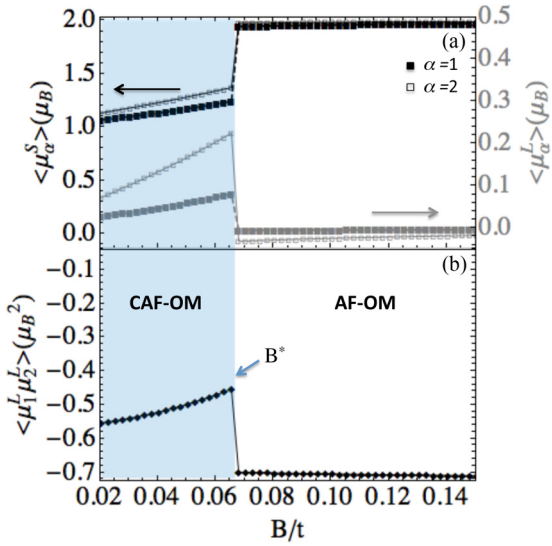

FIG. 2. Evolution of (a) the spin and orbital components of the Ru magnetic density and (b) the Ru-Ru nonlocal orbital moment correlations projected along the c axis. B is the amplitude of the applied Zeeman field oriented along the c axis. We assume that $t = 0.4$ eV, $\Delta_1/t = -0.3$, $\Delta_2/t = 0.225$, $U/t = 5.0$, $J_H/U = 0.2$. AF-OM (CAF-OM) stands for a ferromagnetic ground state with antialigned orbital moments and inequivalent resulting orbital polarization with an averaged amplitude $\mu^L_{av} = (1/2)\,(\langle\mu^L_1\rangle + \langle\mu^L_2\rangle)$ that is smaller (larger) than 0.1. B^* indicates the amplitude of the Zeeman field above (below) which the ground state is spin polarized with a smaller (larger) averaged orbital moment than a given reference that is set at 0.1.

the regime of intermediate electronic correlations set by $U/t = 5.0$ [37]. Concerning the SOC term, we assume an amplitude $\lambda/t = 0.14$ in the range of values that is expected to hold for Sr-based ruthenates [38].

We study the evolution towards the FM state as a function of an applied Zeeman field B (coupled to the spin and orbital angular momenta at the Ru site) along the c axis to assess the relation between the amplitude of the local spin and orbital magnetic moment and the nearest-neighbor orbital pattern. In Fig. 2(a) we present the field dependence of the c-axis projection of the local spin, $\langle\mu^S\rangle$, and orbital, $\langle\mu^L\rangle$, components of the magnetic density evaluated at the Ru_1 and Ru_2 sites. We also track the evolution of the nonlocal orbital correlations between the orbital moments at the two Ru sites $\langle\mu^L_1\mu^L_2\rangle$ [Fig. 2(b)]. The analysis is performed for a representative distortive state of the octahedra at the Ru_1 and Ru_2 sites being in flat and elongated configurations, respectively. There are various remarkable aspects of the correlated spin-polarized state that the presented investigation unveils. First, as one would expect, we observe that inequivalent octahedral distortions generally lead to different spin and orbital magnetic moments at the corresponding Ru sites. We have to recall that the orbital degree of freedom in the d^4 Ru configuration is set by the position of the double occupancy (doublon) within the three t_{2g} orbital states. Then, since flat (elongated) octahedra tend to favor an orbital occupancy with the doublon placed in the xy ($\{xz, yz\}$) orbital sector, one has that the spin-orbit lifting of the orbital degeneracy leads to an orbital magnetic moment which is preferably oriented in the ab plane (c axis). As we can see in Fig. 2, the increase of the applied magnetic field drives the transition between two distinct spin and orbital configurations. At low fields the ground state, labeled canted antiferro-orbital moment (CAF-OM) phase, exhibits a nonsaturated local spin moment $\langle\mu^S\rangle \sim 1$ on both Ru_1 and Ru_2 and an orbital component whose amplitude $\langle\mu^L\rangle$ is comparable to the spin density at the Ru_2 site (elongated octahedron). On the other hand, the Ru-Ru orbital correlations are negative, thus indicating that the orbital moments are antialigned. The amplitude of $\langle\mu^L_1\mu^L_2\rangle$ does not reach the maximal value of -1 in the CAF-OM, and thus, it shows a sort of canting in the orbital configuration.

A further growth of the applied field brings the transition to the fully polarized FM spin state, where the averaged orbital moment over the two Ru sites is suppressed. Indeed, as reported in Fig. 2(b), one can single out an effective amplitude of the Zeeman field B^* that separates the CAF-OM state from the AF-OM one, characterized by a reduced averaged orbital moment $\mu^L_{av} = (1/2)(\langle\mu^L_1\rangle + \langle\mu^L_2\rangle)$, lower than the reference amplitude of $\mu^L_{av} = 0.1$. The microscopic mechanism which governs the quenching of the orbital moment can be understood as follows: when an electron hops between neighboring sites in the spin-polarized background, the effective transfer integral between the degenerate (d_{zx}, d_{yz}) orbitals is optimized if an antiferro-orbital (AFO) configuration is realized, where the double occupancy sits on alternating orbitals on neighboring sites. Such an orbital configuration results in a vanishing value of the average angular momentum density.

To assess the relation between the critical field amplitude B^* and the character of the octahedral distortions, we explored the impact of the variation of the CF potential on the ground state. In particular, we keep in mind that recent studies revealed that distinct structural mechanisms are associated with the c-axis magnetization, specifically an induced extension of the c axis, which may result in an elongation of the apical RuO bonds and a contraction of the in-plane RuO bonds [23]. In our calculations, we mimic this trend by lowering the CF term at the Ru_1 site by keeping fixed the configuration at the Ru_2 site.

In Fig. 3, we report the evolution of the CAF-OM and AF-OM phases as a function of Δ_1 by moving from the zero-field compressed octahedral state ($\Delta_1/t \sim -1.2$) towards the symmetric configuration ($\Delta_1/t = 0$). We do observe that, when the flattening at the Ru_1 site is released by simulating a weakly distorted octahedron ($\Delta_1/t \sim 0$), the FM state with a vanishing orbital moment is settled at lower fields and holds at any amplitude of the applied magnetic field.

Finally, it is worth pointing out that the main objective of the performed computation is to unveil the mechanisms that can account for the observed orbital quenching. Given the cluster size of the quantum simulation and the many competing energy scales in the problem, a tight quantitative correspondence between the theoretical outcome and the experimental data is naturally beyond the scope of the effective model. Still, our analysis is more suitable to single out the range of the microscopic parameters where reasonable qualitative and quantitative agreement on the trend and evolution of the physical observables can be achieved. From this point of view, the specific choice of the Coulomb interaction

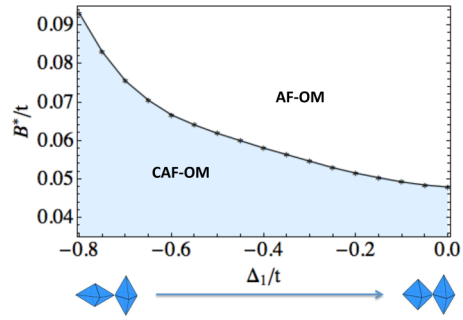

FIG. 3. Evolution of the AF-OM and CAF-OM ferromagnetic phases as a function of the c axis Zeeman field and of the octahedral distortions at the Ru_1 site Δ_1 for a given amplitude of the CF potential (elongated configuration) at Ru_2. B is the amplitude of the applied magnetic field. We assume that $t = 0.4$ eV, $\Delta_1/t = -0.3$, $U/t = 5.0$, $J_H/U = 0.2$. AF-OM (CAF-OM) stands for a ground state with antialigned orbital moments and inequivalent resulting orbital polarization corresponding to an averaged amplitude $\mu^L_{av} = (1/2)\,(\langle\mu^L_1\rangle + \langle\mu^L_2\rangle)$ that is smaller (larger) than 0.1. B^* indicates the amplitude of the Zeeman field above (below) which the ground state is spin polarized with a smaller (larger) averaged orbital moment than a given reference that is set at 0.1.

parameters, U and J_H, is not crucial. However, the disentangling of spin and orbital degrees of freedom by the applied magnetic field along c, which drives magnetic ordering coexisting with short-range antiferro-orbital correlations, can be obtained only in a correlated picture. We expect that the outcomes will not be qualitatively altered when considering other correlated approaches with embedded (e.g., dynamical field theory) or coupled clusters (e.g., cluster perturbation methods) to deal with the full lattice problem.

V. CONCLUSIONS

We used polarized neutron scattering diffraction to determine the spin and orbital character of the magnetic state of $Sr_4Ru_3O_{10}$ in the high-field FM phase with spin moments aligned along the c axis. Remarkably, our study revealed a vanishing contribution of the orbital component to the magnetic density at Ru sites. We discussed the microscopic mechanisms which are able to account for the suppression of the orbital moment as being due to the formation of robust antiferro-orbital correlations which are driven by the fully polarized magnetic FM phase. Moreover, we showed that such a microscopic mechanism may be assisted by the structural deformations (namely, expansion of the apical Ru-O distances of inner and outer octahedra) which effectively separate the planar d_{xy} bands from the longitudinal (d_{xz}, d_{yz}) doublet and are allowed in a certain window for the CF parameters which simulate the tetragonal deformations. In particular, we showed that the effective magnetic field to access the FM phase with a vanishing orbital moment is lower in the case where the octahedra are more uniform and less compressed along the c axis.

The comprehensive view offered by the comparative studies of the field-induced magnetic phases of $Sr_4Ru_3O_{10}$, for longitudinal and in-plane applied fields, highlights the role of the orbital component in setting the anisotropic magnetic response. In particular, we provided a self-contained physical scenario where the orbital moment is suppressed when the field is applied along the c axis, while it is substantial and at the origin of the layer-dependent magnetic response in the case of an in-plane applied field.

ACKNOWLEDGMENTS

We acknowledge insightful discussions with and valuable support during the experiments by A. Stunault, O. Fabelo, A. J. Rodriguez Velamazan, and A. Goukassov.

APPENDIX: MODEL HAMILTONIAN

In this Appendix, we report the details of the model Hamiltonian employed to simulate the evolution of the spin and orbital angular momentum in a cluster consisting of two inequivalent Ru sites.

The examined microscopic model Hamiltonian with two inequivalent atoms, Ru_1 and Ru_2, is expressed as

$$H = H_{\rm kin} + H_{\rm el-el} + H_{\rm cf} + H_{\rm soc} + H_z. \tag{A1}$$

The first term in Eq. (A1) is the kinetic operator between the t_{2g} orbitals on different Ru sites,

$$H_{\rm kin} = -t \sum_{ij,\sigma\alpha} (d^\dagger_{i\alpha\sigma} d_{j\alpha\sigma} + \text{H.c.}), \tag{A2}$$

with $d^\dagger_{i\alpha\sigma}$ being the creation operator for an electron with spin σ at the i site in the α orbital. A similar modeling approach is commonly adopted to describe the kinetic term in transition metal compounds with partially filled d-bands having different orbital character [39,40]. The second term is the local Coulomb interaction between t_{2g} electrons [34,41]:

$$H_{\rm el-el} = U \sum_{i\alpha} n_{i\alpha\uparrow} n_{i\alpha\downarrow} - 2J_H \sum_{i\alpha\beta} \mathbf{S}_{i\alpha} \cdot \mathbf{S}_{i\beta} + \left(U' - \frac{J_H}{2}\right) \sum_{i\alpha\neq\beta} n_{i\alpha} n_{i\beta} + J' \sum_{i\alpha\beta} d^\dagger_{i\alpha\uparrow} d^\dagger_{i\alpha\downarrow} d_{i\beta\uparrow} d_{i\beta\downarrow}, \tag{A3}$$

where $n_{i\alpha\sigma}$ and $\mathbf{S}_{i\alpha}$ are the on-site charge for spin σ and the spin operators for the α orbital, respectively. U (U') is the intraorbital (interorbital) Coulomb repulsion, J_H is Hund's coupling, and J' is the pair-hopping term. Due to the invariance for rotations in the orbital space, the following relations hold: $U = U' + 2J_H$, $J' = J_H$.

The $H_{\rm cf}$ part of the Hamiltonian H is the crystalline field potential, controlling the symmetry lowering from the cubic to tetragonal one:

$$H_{\rm cf} = \sum_i \Delta_i \left[n_{ixy} - \frac{1}{2}(n_{ixz} + n_{iyz}) \right]. \tag{A4}$$

The SOC Hamiltonian reads

$$H_{\rm soc} = \lambda \sum_i \mathbf{L}_i \cdot \mathbf{S}_i. \tag{A5}$$

Due to the cubic CF terms in RuO_6 octahedra separating the lower t_{2g} from the unoccupied e_g levels, $\mathbf{L}_i$ stands for an effective $L = 1$ angular momentum, projected onto the t_{2g}

subspace. Its components have the following expression in terms of orbital fermionic operators:

$$L_{iz} = i\sum_{\sigma}[d^{\dagger}_{ixz\sigma}d_{iyz\sigma} - d^{\dagger}_{iyz\sigma}d_{ixz\sigma}],$$
$$L_{ix} = i\sum_{\sigma}[d^{\dagger}_{ixy\sigma}d_{ixz\sigma} - d^{\dagger}_{ixz\sigma}d_{ixy\sigma}],$$
$$L_{iy} = i\sum_{\sigma}[d^{\dagger}_{iyz\sigma}d_{ixy\sigma} - d^{\dagger}_{ixy\sigma}d_{iyz\sigma}]. \quad \text{(A6)}$$

The SOC term binds $\mathbf{L}_i$ and spin $\mathbf{S}_i$ momenta into the total angular momentum $\mathbf{J}_i = \mathbf{L}_i + \mathbf{S}_i$. Although the spin-orbit term commutes with both total angular momenta $\mathbf{J}_i^2$ and J_i^z, the full Hamiltonian of Eq. (A1) has a reduced symmetry, for J_i^z is not a conserved quantity due to the orbital anisotropy of the kinetic term [42]. Since the total angular momentum does not provide a good quantum description, we consider the $\mathbf{S}_i$ and $\mathbf{L}_i$ operators and evaluate the corresponding average expectation values to fully characterize the spin and orbital character of the ground state.

Finally, H_z in Eq. (A1) describes the Zeeman coupling of the local angular momenta to a magnetic field B applied along the c symmetry direction, expressed in units of the Bohr magneton:

$$H_z = \sum_i (\mathbf{L}_i + 2\mathbf{S}_i)\cdot\mathbf{B}_z. \quad \text{(A7)}$$

[1] M. Malvestuto, E. Carleschi, R. Fittipaldi, E. Gorelov, E. Pavarini, M. Cuoco, Y. Maeno, F. Parmigiani, and A. Vecchione, Phys. Rev. B **83**, 165121 (2011).

[2] A. P. Mackenzie and Y. Maeno, Rev. Mod. Phys. **75**, 657 (2003).

[3] J. Lee, M. P. Allan, M. A. Wang, J. Farrel, S. A. Grigera, F. Baumberger, J. C. Davis, and A. P. Mackenzie, Nat. Phys. **5**, 800 (2009).

[4] X. N. Lin, Z. X. Zhou, V. Durairaj, P. Schlottmann, and G. Cao, Phys. Rev. Lett. **95**, 017203 (2005).

[5] Z. Q. Mao, M. Zhou, J. Hooper, V. Golub, and C. J. O'Connor, Phys. Rev. Lett. **96**, 077205 (2006).

[6] G. Cao, L. Balicas, W. H. Song, Y. P. Sun, Y. Xin, V. A. Bondarenko, J. W. Brill, S. Parkin, and X. N. Lin, Phys. Rev. B **68**, 174409 (2003).

[7] H. T. Jeng, S. H. Lin, and C. S. Hsue, Phys. Rev. Lett. **97**, 067002 (2006).

[8] T. F. Qi, O. B. Korneta, L. Li, K. Butrouna, V. S. Cao, X. Wan, P. Schlottmann, R. K. Kaul, and G. Cao, Phys. Rev. B **86**, 125105 (2012).

[9] Y. Cao, Q. Wang, J. A. Waugh, T. J. Reber, H. Li, X. Zhou, S. Parham, S.-R. Park, N. C. Plumb, E. Rotenberg, A. Bostwick, J. D. Denlinger, T. Qi, M. A. Hermele, G. Cao, and D. S. Dessau, Nat. Commun. **7**, 11367 (2016).

[10] H. Lei, W.-G. Yin, Z. Zhong, and H. Hosono, Phys. Rev. B **89**, 020409(R) (2014).

[11] F. Forte, M. Cuoco, and C. Noce, Phys. Rev. B **82**, 155104 (2010).

[12] C. Bergemann, A. P. Mackenzie, S. R. Julian, D. Forsythe, and E. Ohmichi, Adv. Phys. **52**, 639 (2003).

[13] D. Sutter, C. G. Fatuzzo, S. Moser, M. Kim, R. Fittipaldi, A. Vecchione, V. Granata, Y. Sassa, F. Cossalter, G. Gatti, M. Grioni, H. M. Ronnow, N. C. Plumb, C. E. Matt, M. Shi, M. Hoesch, T. K. Kim, T. R. Chang, H. T. Jeng, C. Jozwiak, A. Bostwick, E. Rotenberg, A. Georges, T. Neupert, and J. Chang, Nat. Commun. **8**, 15176 (2017).

[14] L. Das, F. Forte, R. Fittipaldi, C. G. Fatuzzo, V. Granata, O. Ivashko, M. Horio, F. Schindler, M. Dantz, Y. Tseng, D. E. McNally, H. M. Ronnow, W. Wan, N. B. Christensen, J. Pelliciari, P. Olalde-Velasco, N. Kikugawa, T. Neupert, A. Vecchione, T. Schmitt, M. Cuoco, and J. Chang, Phys. Rev. X **8**, 011048 (2018).

[15] D. G. Porter, V. Granata, F. Forte, S. Di Matteo, M. Cuoco, R. Fittipaldi, A. Vecchione, and A. Bombardi, Phys. Rev. B **98**, 125142 (2018).

[16] R. S. Perry, L. M. Galvin, S. A. Grigera, L. Capogna, A. J. Schofield, A. P. Mackenzie, M. Chiao, S. R. Julian, S. I. Ikeda, S. Nakatsuji, Y. Maeno, and C. Pfleiderer, Phys. Rev. Lett. **86**, 2661 (2001).

[17] R. A. Borzi, S. A. Grigera, J. Farrell, R. S. Perry, S. J. S. Lister, S. L. Lee, D. A. Tennant, Y. Maeno, and A. P. Mackenzie, Science **315**, 214 (2007).

[18] M. Malvestuto, V. Capogrosso, E. Carleschi, L. Galli, E. Gorelov, E. Pavarini, R. Fittipaldi, F. Forte, M. Cuoco, A. Vecchione, and F. Parmigiani, Phys. Rev. B **88**, 195143 (2013).

[19] B. Binz and M. Sigrist, Europhys. Lett. **65**, 816 (2004).

[20] H. Yamase and A. A. Katanin, J. Phys. Soc. Jpn. **76**, 073706 (2007).

[21] C. Autieri, M. Cuoco, and C. Noce, Phys. Rev. B **85**, 075126 (2012).

[22] V. Granata, L. Capogna, M. Reehuis, R. Fittipaldi, B. Ouladdiaf, S. Pace, M. Cuoco, and A. Vecchione, J. Phys. Condens. Matter **25**, 056004 (2013).

[23] W. Schottenhamel, M. Abdel-Hafiez, R. Fittipaldi, V. Granata, A. Vecchione, M. Hücker, A. U. B. Wolter, and B. Büchner, Phys. Rev. B **94**, 155154 (2016).

[24] F. Weickert, L. Civale, B. Maiorov, M. Jaime, M. B. Salamon, E. Carleschi, A. M. Strydom, R. Fittipaldi, V. Granata, and A. Vecchione, Sci. Rep. **7**, 3867 (2017).

[25] V. Granata, L. Capogna, F. Forte, M.-B. Lepetit, R. Fittipaldi, A. Stunault, M. Cuoco, and A. Vecchione, Phys. Rev. B **93**, 115128 (2016).

[26] R. Fittipaldi, D. Sisti, A. Vecchione, and S. Pace, Cryst. Growth Des. **7**, 2495 (2007).

[27] E. Carleschi, B. P. Doyle, R. Fittipaldi, V. Granata, A. M. Strydom, M. Cuoco, and A. Vecchione, Phys. Rev. B **90**, 205120 (2014).

[28] G. L. Squires, *Introduction to the Theory of Thermal Neutron Scattering* (Cambridge University Press, Cambridge, 1978).

[29] E. Prince (ed.), *International Tables for Crystallography*, Vol. C, Mathematical, Physical and Chemical Tables (Springer, Dordrecht, 2006).
[30] J. Rodriguez Carvajal, Phys. B (Amsterdam, Neth.) **192**, 55 (1993).
[31] M. K. Crawford, R. L. Harlow, W. Marshall, Z. Li, G. Cao, R. L. Lindstrom, Q. Huang, and J. W. Lynn, Phys. Rev. B **65**, 214412 (2002).
[32] K. Momma, T. Ikeda, A. A. Belik, and F. Izumi, Powder Diffr. **28**, 184 (2013).
[33] D. J. Singh and I. I. Mazin, Phys. Rev. B **63**, 165101 (2001).
[34] M. Cuoco, F. Forte, and C. Noce, Phys. Rev. B **73**, 094428 (2006).
[35] E. Dagotto, Rev. Mod. Phys. **66**, 763 (1994).
[36] D. Pincini, L. S. I. Veiga, C. D. Dashwood, F. Forte, M. Cuoco, R. S. Perry, P. Bencok, A. T. Boothroyd, and D. F. McMorrow, Phys. Rev. B **99**, 075125 (2019).
[37] E. Gorelov, M. Karolak, T. O. Wehling, F. Lechermann, A. I. Lichtenstein, and E. Pavarini, Phys. Rev. Lett. **104**, 226401 (2010).
[38] M. W. Haverkort, I. S. Elfimov, L. H. Tjeng, G. A. Sawatzky, and A. Damascelli, Phys. Rev. Lett. **101**, 026406 (2008).
[39] C. Autieri, G. Cuono, F. Forte, and C. Noce, J. Phys.: Condens. Matter **29**, 224004 (2017).
[40] C. Autieri, G. Cuono, F. Forte, and C. Noce, J. Phys.: Conf. Ser. **969**, 012106 (2018).
[41] M. Cuoco, F. Forte, and C. Noce, Phys. Rev. B **74**, 195124 (2006).
[42] W. Brzezicki, A. M. Oles, and M. Cuoco, Phys. Rev. X **5**, 011037 (2015).